Broken symmetry and quantum entanglement of an exciton in $In_xGa_{1-x}As/GaAs$ quantum dot molecules

Gabriel Bester and Alex Zunger
National Renewable Energy Laboratory, Golden, Colorado 80401, USA

J. Shumway
Department of Physics and Astronomy, Arizona State University, Tempe, Arizona 85287-1504

(Received 29 June 2004; revised manuscript received 10 November 2004; published 25 February 2005; corrected 2 March 2005)

The ability of a quantum dot to confine photogenerated electron-hole pairs created interest in the behavior of such an exciton in a "dot molecule," being a possible register in quantum computing. When two quantum dots are brought close together, the quantum state of the exciton may extend across both dots. The exciton wave function in such a dot molecule may exhibit entanglement. Atomistic pseudopotential calculations of the wave function for an electron-hole pair in a dot molecule made of two identical $In_xGa_{1-x}As/GaAs$ dots reveal that the common assumption of single-particle wave functions forming bonding and antibonding states is erroneous. The true behavior of single-particle electrons and holes leads to symmetry-broken excitonic two-particle wave functions, dramatically suppressing entanglement. We find that at large interdot separations, the exciton states are built from heteronuclear single-particle states while at small interdot separations the exciton is derived from heteronuclear hole states and homonuclear electron states. We calculate the entanglement of the excitons and find a maximum value of 80% at an interdot separation of 8.5 nm and very small values for larger and smaller distances.

DOI: 10.1103/PhysRevB.71.075325 PACS number(s): 78.67.Hc, 73.21.La, 03.67.Mn

I. INTRODUCTION

A. Entanglement of an exciton in a molecule

Unlike its classical counterpart, a *quantum bit* (qubit) *A* can exist not only in the two states "0" and "1," but in a linear combination of states: $|\Psi_A\rangle=\alpha|0_A\rangle+\beta|1_A\rangle$ in a two-dimensional Hilbert space. Accordingly, a pair of qubits *A* and *B* can exist in a superposition of the four basis states $|0_A0_B\rangle$, $|0_A1_B\rangle$, $|1_A0_B\rangle$, and $|1_A1_B\rangle$. The most important correlated qubit states in quantum computation and quantum information[1–3] are the maximally entangled (Bell) states $|\Psi_{AB}\rangle=(1/\sqrt{2})\{|0_A0_B\rangle\pm|1_A1_B\rangle\}$, which allow quantum algorithms to outperform classical algorithms.[1–3] Semiconductor quantum dots confine electrons and holes in discrete energy levels a few nanometers in size.[4] These properties have driven speculation that quantum dots may provide physical realization of qubits. Proposed implementations using quantum dots include the presence versus absence of an electron in a certain dot level,[5–7] the spin-up versus spin-down state of an electron,[1,8–10] or the presence of an electron or a hole in one dot versus another dot.[11–14] An implementation of the latter proposition has been made possible by the ability to grow pairs of vertically coupled self-assembled quantum dots with varying separations.[15,16] This has offered the possibility of creating a *register* of two qubits *A* and *B* in the two basis states top dot (*T*) and bottom dot (*B*). A relatively simple proposal is to use as qubit *A* the electron and as qubit *B* the hole of an electron-hole pair (*e-h*, created by light excitation[11]) where the two qubits can be in the states "top" (*T*) and "bottom" (*B*) of the dot molecule. The so-defined two qubits could form entangled as well as unentangled states. One first considers the *single-particle* electron and hole orbitals (analogous to molecular orbitals in H_2^+) which form bonding and antibonding combinations:

$$\phi_h^{\text{bonding}}=\frac{1}{\sqrt{2}}(h_T+h_B),\quad \phi_h^{\text{anti}}=\frac{1}{\sqrt{2}}(h_T-h_B),$$

$$\phi_e^{\text{bonding}}=\frac{1}{\sqrt{2}}(e_T+e_B),\quad \phi_e^{\text{anti}}=\frac{1}{\sqrt{2}}(e_T-e_B), \qquad (1)$$

where e_T (e_B) represents an electron in the top (bottom) dot; h_T (h_B) represents a hole in the top (bottom) dot. When the interparticle Coulomb interaction is introduced, these single-particle states can form correlated excitons. *Unentangled* excitons form from simple direct products—e.g., $\phi_e^{\text{bonding}}\otimes\phi_h^{\text{bonding}}=\frac{1}{2}(e_Th_T+e_Bh_B+e_Th_B+e_Bh_T)$—and thus contain terms due to an *e-h* pair in a single dot, as well as terms due to an electron in one dot and a hole in another. In contrast, the *maximally entangled* states form from sums and differences of simple direct products containing either *e-h* pair in one dot or dissociated states, but not both[11]:

$$|a\rangle=\frac{1}{\sqrt{2}}\{|e_Bh_B\rangle+|e_Th_T\rangle\},\quad \text{bound exciton, bonding,}$$

$$|d\rangle=\frac{1}{\sqrt{2}}\{|e_Bh_B\rangle-|e_Th_T\rangle\},\quad \text{bound exciton, antibonding,}$$

$$|c\rangle=\frac{1}{\sqrt{2}}\{|e_Bh_T\rangle-|e_Th_B\rangle\},\quad \text{dissociated, antibonding,}$$

$$|b\rangle=\frac{1}{\sqrt{2}}\{|e_Bh_T\rangle+|e_Th_B\rangle\},\quad \text{dissociated, bonding.} \qquad (2)$$

Bayer *et al.*[11] and Korkusinski *et al.*[14] formulated simple models for the energies of the four excitons starting from Eq. (2) in a double dot and compared the predicted energies with experiment. Experimentally, the emission spectra of a dot molecule showed[11,14] two exciton transitions separated by an energy ΔE. This energy ΔE was shown to increase with decreasing interdot separation. This observation was in agreement with the theory where the same behavior was obtained. However, we will show that in this case the agreement between experiment and theory does not necessarily validate the theoretical assumption. We offer here a fundamental theory of dot molecules based on a fully atomistic approach. Our results differ significantly from those of Bayer *et al.*[11] and Korkusinski *et al.*,[14] in that we predict a reduced exciton energy in a dot molecule relative to isolated dots (the simple models predict an enhanced energy) and that entanglement is generally weak (the simple models predict high entanglement). In what follows we first introduce simple models which will serve to explain previous results (Sec. I B). Following this we will describe our fully atomistic results.

B. Simple models describing an exciton in a dot molecule

Before displaying our method and results, we briefly describe the expectations from a simple model. This will serve to describe the main assumption of Bayer *et al.*[11] and Korkusinski *et al.*[14] and clarify the basis of more general approaches.

In order to decide weather to expect unentangled or entangled excitons in a system of two interacting quantum dots one could attempt to use a two-site tight-binding Hamiltonian with intuitively chosen parameters. The basis for this Hamiltonian can be constructed from products of the electron and hole single-particle states $|e_T h_T\rangle$, $|e_T h_B\rangle$, $|e_B h_T\rangle$, and $|e_B h_B\rangle$. The two-site Hamiltonian in this basis is given by

$$H = \begin{pmatrix} \varepsilon_e^T - \varepsilon_h^T + U_{eh}^{TT} & t_e & t_h & 0 \\ t_e & \varepsilon_e^B - \varepsilon_h^T + U_{eh}^{BT} & 0 & t_h \\ t_h & 0 & \varepsilon_e^T - \varepsilon_h^B + U_{eh}^{TB} & t_e \\ 0 & t_h & t_e & \varepsilon_e^B - \varepsilon_h^B + U_{eh}^{BB} \end{pmatrix}, \tag{3}$$

where $\{\varepsilon_e^T, \varepsilon_e^B, \varepsilon_h^T, \varepsilon_h^B\}$ are the electron and hole on-site energies, $\{t_e, t_h\}$ are the hopping matrix elements, and $\{U_{eh}^{TT}, U_{eh}^{TB}, U_{eh}^{BT}, U_{eh}^{BB}\}$ are the electron-hole Coulomb matrix elements. Different assumptions can be made here, leading to two models.

1. Model 1: $\varepsilon_h^T = \varepsilon_h^B$, $\varepsilon_e^T = \varepsilon_e^B$, $t_e = t_h$, $U = 0$

A simple trial assumption is to assumed (i) that the two dots T and B forming the molecule have identical on-site single-particle energies $\varepsilon_h^T = \varepsilon_h^B$ and $\varepsilon_e^T = \varepsilon_e^B$, (ii) the hoping matrix elements for electrons and holes are identical: $t_e = t_h$, (iii) the electron-hole Coulomb matrix elements U_{eh} are negligible. The single-particle electron and hole energy levels for this case are schematically shown in Fig. 1(a) where the electron and hole levels e_0, e_1 and h_0, h_1 form bonding and antibonding combinations as in Eq. (1), so the energies split symmetrically as a function of interdot separation. The *excitonic* electron-hole eigenvectors of the Hamiltonian in Eq. (3) are given in order of increasing energy by

$$|1\rangle = \frac{1}{2}\{|e_T h_T\rangle - |e_B h_T\rangle - |e_T h_B\rangle + |e_B h_B\rangle\},$$

$$|2\rangle = \frac{1}{\sqrt{2}}\{|e_B h_B\rangle - |e_T h_T\rangle\},$$

$$|3\rangle = \frac{1}{\sqrt{2}}\{|e_B h_T\rangle - |e_T h_B\rangle\},$$

$$|4\rangle = \frac{1}{2}\{|e_T h_T\rangle + |e_B h_T\rangle + |e_T h_B\rangle + |e_B h_B\rangle\}. \tag{4}$$

Excitons $|1\rangle$ and $|4\rangle$ are symmetric and therefore optically active (bright) while $|2\rangle$ and $|3\rangle$ are energetically degenerate and optically dark. If we further assume that the hopping matrix elements t_e and t_h increase when the interdot distance is reduced, we find the spectrum depicted in Fig. 2(a). The

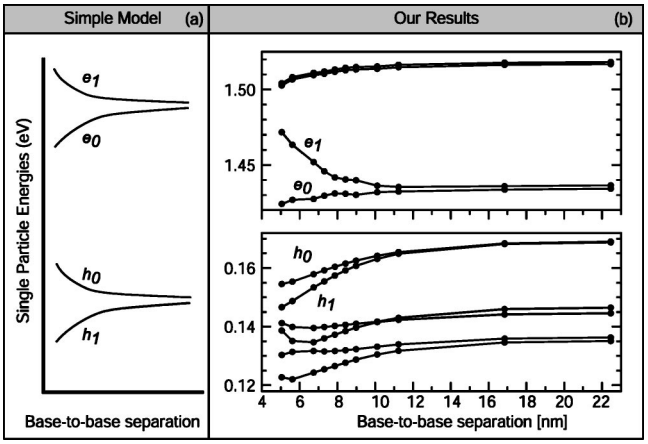

FIG. 1. Single-particle energies assumed in models 1 and 2 [panel (a)] and results from our pseudopotential calculations [panel (b)]. The reference energy for our results is set to the unstrained valence-band maximum of GaAs.

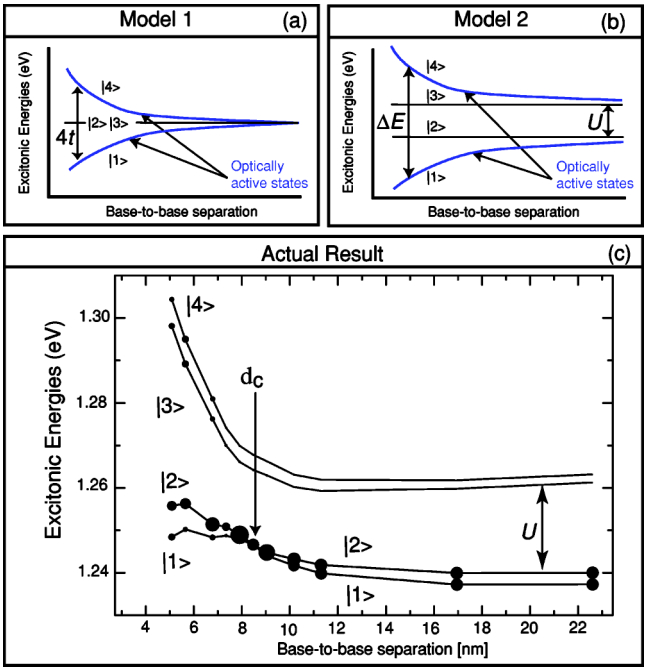

FIG. 2. (Color online) Exciton energies as a function of the interdot separation for two different models (models 1 and 2) and for our pseudopotential-CI results (actual results). The circles on the excitonic lines of the lower panel are proportional to the oscillator strength of the transitions.

two bright states $|1\rangle$ and $|4\rangle$ move energetically apart, where the energy of state $|1\rangle$ decreases by $2t$ while the energy and state $|4\rangle$ increases by $2t$ with decreasing interdot separation. This qualitative behavior resembles the experimental observation[14,17] where two peaks move apart and one could be tempted to fit the hopping parameters $t=t_e=t_h$ to the experimental splitting of the bright states. We will show later that this model is in strong disagreement with the underlying physics.

2. Model 2: $\varepsilon_h^T=\varepsilon_h^B$, $\varepsilon_e^T=\varepsilon_e^B$, $t_e=t_h$, $U\neq 0$

A slightly more realistic model, similar to the one presented in Refs. 11 and 14, uses a different assumption for (iii), taking Coulomb attraction into account. Here the electron-hole Coulomb energies $U_{eh}^{TT}=U_{eh}^{BB}$ for the *exciton* states, where both the electron and hole reside on the same dot, are assumed to be larger than the Coulomb elements of the *dissociated exciton* $U_{eh}^{TB}=U_{eh}^{BT}$, where the electron and hole are located on different dots. Setting $U_{eh}^{TT}=U_{eh}^{BB}=U$ and $U_{eh}^{TB}=U_{eh}^{BT}=0$ in the Hamiltonian from Eq. (3) yields in increasing order of energy the four exciton states $|1\rangle$, $|2\rangle$, $|3\rangle$, and $|4\rangle$:

$$|1\rangle=\frac{1}{\sqrt{2(1+\gamma_1^2)}}\{|e_Th_T\rangle+|e_Bh_B\rangle-\gamma_1(|e_Bh_T\rangle+|e_Th_B\rangle)\},$$

$$|2\rangle=\frac{1}{\sqrt{2}}\{|e_Bh_B\rangle-|e_Th_T\rangle\},$$

$$|3\rangle=\frac{1}{\sqrt{2}}\{|e_Bh_T\rangle-|e_Th_B\rangle\},$$

$$|4\rangle=\frac{1}{\sqrt{2(1+\gamma_2^2)}}\{|e_Th_T\rangle+|e_Bh_B\rangle-\gamma_2(|e_Bh_T\rangle+|e_Th_B\rangle)\}, \tag{5}$$

with

$$\gamma_1=\frac{U+\sqrt{(4t)^2+U^2}}{4t},\quad \gamma_2=\frac{U-\sqrt{(4t)^2+U^2}}{4t}. \tag{6}$$

Their eigenvalues are given by

$$E_1=\varepsilon_e-\varepsilon_h+\frac{1}{2}U-\frac{1}{2}\sqrt{(4t)^2+U^2},$$

$$E_2=\varepsilon_e-\varepsilon_h-U,$$

$$E_3=\varepsilon_e-\varepsilon_h,$$

$$E_4=\varepsilon_e-\varepsilon_h+\frac{1}{2}U+\frac{1}{2}\sqrt{(4t)^2+U^2}. \tag{7}$$

We obtain two antisymmetric (dark) states $|2\rangle$ and $|3\rangle$ that are fully entangled (Bell) states. The states $|1\rangle$ and $|4\rangle$ cannot be written as simple direct products and are, to some degree, entangled. The limiting case of vanishing Coulomb ($U\rightarrow 0$) interaction gives, as expected from model 1, the states $|1\rangle$, $|2\rangle$, $|3\rangle$, and $|4\rangle$ from Eq. (4) where $|1\rangle$ and $|4\rangle$ are unentangled. The case for nonzero but small hopping elements ($t\rightarrow 0$) gives for $|1\rangle$, $|2\rangle$, $|3\rangle$, and $|4\rangle$ the eigenstates $|b\rangle$, $|d\rangle$, $|c\rangle$, and $|a\rangle$, respectively, from Eqs. (2) which are all fully entangled states. The states $|1\rangle$ and $|4\rangle$ are bright while $|2\rangle$ and $|3\rangle$ are dark. An increasing value of t introduces a mixing between the states $|1\rangle$ and $|4\rangle$; these states change character and have presumably lower entanglement, while the states $|2\rangle$ and $|3\rangle$ remain dark and fully entangled. The energetic evolution of the states $|1\rangle$, $|2\rangle$, $|3\rangle$, and $|4\rangle$ with decreasing interdot separation is given in Fig. 2(b). The energy separation between the two bright states $|1\rangle$ and $|4\rangle$ is $\Delta E=\sqrt{(4t)^2+U^2}$. At large interdot separation, $|1\rangle$ and $|3\rangle$ as well as $|2\rangle$ and $|4\rangle$ are energetically degenerate. Both doublets are separated by U. The excitonic wave functions $|1\rangle$, $|2\rangle$, $|3\rangle$, and $|4\rangle$ are illustrated schematically on the right-hand side of Fig. 3 for large interdot separation (large-d case) and small interdot separation (small-d case). Again, the result of two bright states $|1\rangle$ and $|4\rangle$ moving energetically apart with decreasing interatomic distance is in agreement with experiment, spurring hope that the theoretically predicted high degree of entanglement in this system could be experimentally realized[11,14] to the benefit of quantum computing.

However, there are reasons to doubt the validity of the simple diatomiclike analog of dot molecules, since actual self-assembled quantum dots contain tens of thousands of atoms and the dots themselves are strained by the host matrix and submitted to random alloy fluctuations. Indeed, the electronic properties of such dots depend on their shape, size, composition profile, and strain profile[18] and cannot,[19] for in-

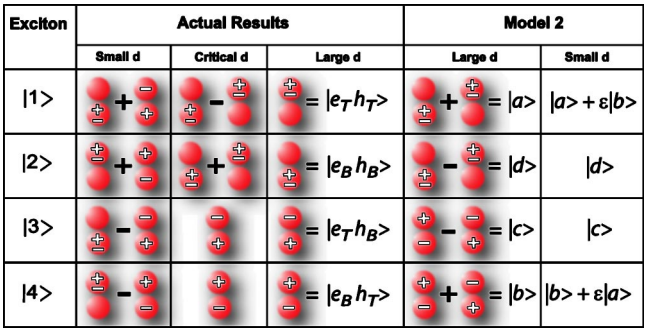

FIG. 3. Schematic representation of the excitonic wave functions obtained from our pseudopotential CI calculations (left) and in the simple model presented in the introduction (right). The symbols are + (hole), − (electron), or ± (exciton). The two spheres denote top and bottom dots. The value of the critical distance is 8.5 nm for our specific case.

stance, be modeled by simple single-band effective-mass models. Furthermore, the assumption $t_e = t_h$ is very questionable given the large mass ratio $m_e/m_{hh} \approx 0.06/0.40 \approx 1/6$ of electrons and heavy holes in the GaAs barrier between the dots. Indeed, coupling between a larger number of bands than afforded by simplistic models, and consideration of the strain field between the dots could prevent effective tunneling of either electrons or holes. Thus, a more complete theoretical treatment is called for.

In the present work we study entanglement in dot molecules, using the pseudopotential many-body approach, previously[18,20,21] applied to successfully study many electronic and optical properties of single dots. We consider molecules made of two vertically stacked lens-shaped InGaAs/GaAs dots of identical shape, size, and composition with varying interdot distances. The *single-particle* problem is solved within a multiband, multivalley pseudopotential plane-wave method,[22] including the effects of strain and spin-orbit. The *many-body* problem is solved via a configuration-interaction expansion within the basis of pseudopotential single-particle states. We find that the molecular description of Eq. (1) and Fig. 1(a) breaks down already for the single-particle hole states, which are localized on *one* of the two dots, not forming bonding-antibonding combinations as in Eq. (1). This reflects the fact that the actual potential experienced by holes *in between the dots* is repulsive for its heavy-hole component, and this repulsion is reinforced when the dots are brought together, preventing effective interdot tunneling. This is different from the potential within a real diatomic molecule, which is attractive everywhere, with reinforced attraction when the atoms are brought together. Thus, "artificial dot molecules" behave differently from real molecules, in that the single-particle molecular orbitals demonstrate broken symmetry, akin to heteronuclear molecules (e.g., HF), not homonuclear molecules (H_2). This single-particle symmetry-breaking effects in real dot molecules affects their many-particle excitonic states, which now differ from the maximally entangled model states in Eqs. (4) and (2), exhibiting instead $(|e_B h_B\rangle + |e_T h_B\rangle)$-like behavior with a low degree of entanglement. By varying the interdot separation we predict the many-particle optical spectrum and identify the interdot separation that has the highest degree of entanglement. This establishes an important link between quantum entanglement and the molecular geometry.

II. METHOD

A. Calculation of exciton states

The method of calculation involves two separate steps. In the first step we solve the single-particle Schrödinger equation for a superposition of strain-dependent atomic pseudopotentials $\Sigma_\alpha \Sigma_n v_\alpha(\boldsymbol{r} - \boldsymbol{R}_n)$. These potentials are centered at the relaxed atom positions $\boldsymbol{R}_n$ which are determined using the valence force field method.[23] The atomic pseudopotentials v_α include spin-orbit effects and are fit to InAs and GaAs bulk properties.[24] The single-particle dot molecule wave functions $\psi(\mathbf{r})$ for the CBM electron orbital and level and the VBM hole orbital and level are expanded in terms of strain-dependent Bloch functions $\phi_{n,\mathbf{k}}(\mathbf{r})$:

$$\psi(\boldsymbol{r}) = \sum_{n}^{N_B} \sum_{\mathbf{k}}^{N_k} C_{\boldsymbol{k},n} \phi_{\boldsymbol{k},n}(\boldsymbol{r}), \tag{8}$$

where

$$\phi_{\boldsymbol{k},n}(\boldsymbol{r}) = \frac{1}{\sqrt{N}} u_{\boldsymbol{k},n}(\boldsymbol{r}) e^{i\boldsymbol{k}\cdot\boldsymbol{r}}, \tag{9}$$

with band index n and wave vector $\boldsymbol{k}$ of the underlying bulk solids; the number of primary cells, N; the number of $\boldsymbol{k}$ points, $N_{\mathbf{k}}$; and the number of bands, N_B ["strain-dependent linear combination of bulk bands" (SLCBB) (Ref. 22)].

In the second step we follow the configuration interaction (CI) method and construct a set of Slater determinants.[21]:

$$|\Phi_{h_i,e_j}\rangle = b^\dagger_{h_i} c^\dagger_{e_j} |\Phi_0\rangle, \tag{10}$$

where $b^\dagger_{h_i}$ is the creation operator for holes and $c^\dagger_{e_j}$ the creation operator for electrons. The Slater determinants $|\Phi_{h_i,e_j}\rangle$ can be calculated from antisymmetrized products of single-particle wave functions ψ_i (Ref. 25).

The exciton wave functions $|\Psi\rangle$ are expanded in terms of this determinental basis set:

$$|\Psi\rangle = \sum_{h_i,e_j} A(h_i,e_j) |\Phi_{h_i,e_j}\rangle. \tag{11}$$

The matrix elements of the many-body Hamiltonian involves the calculation of the two center integrals for particle a and particle b:

$$\langle \psi^a_i \psi^b_j | \hat{\mathrm{U}} | \psi^b_{j'}, \psi^a_{i'} \rangle = \int \int \frac{\psi^\star_i(\boldsymbol{r}_a) \psi^\star_j(\boldsymbol{r}_b) \psi_{j'}(\boldsymbol{r}_b) \psi_{i'}(\boldsymbol{r}_a)}{\epsilon(\boldsymbol{r}_a,\boldsymbol{r}_b)|\boldsymbol{r}_a - \boldsymbol{r}_b|} \mathrm{d}\boldsymbol{r}_a \mathrm{d}\boldsymbol{r}_b. \tag{12}$$

The dielectric function ϵ is calculated using the model of Resta.[26]

The shape and size for our dot molecule are inspired from the experimental studies of Bayer *et al.*[11] The dots have a truncated cone shape with 12 nm (bottom) and 10 nm (top) bases and 2 nm height. The composition profile is linear,

starting from $In_{0.5}Ga_{0.5}As$ at the base, to pure InAs at the top of the dots. Both dots have one monolayer wetting layer. The separation between the dots is given as the base-to-base separation d.

B. Method of analysis

The single-particle states can be analyzed by a projection onto valence- and conduction-band states of the bulk at the Γ point:

$$\psi(\boldsymbol{r}) = \frac{1}{\sqrt{N}} \sum_{n}^{N_B} \sum_{\mathbf{k}}^{N_k} C'_{\mathbf{k},n} [u_{\Gamma,n}(\boldsymbol{r}) e^{i\mathbf{k}\cdot\boldsymbol{r}}] \equiv \sum_{n}^{N_B} f_n(\boldsymbol{r}) u_{\Gamma,n}(\boldsymbol{r}), \tag{13}$$

with $f_n(\boldsymbol{r})$ being the envelope functions and

$$C'_{\mathbf{k},n} = \sum_{n'} C_{\mathbf{k},n'} \langle u_{\Gamma,n} | u_{\mathbf{k},n'} \rangle. \tag{14}$$

Once this projection is available we classify the states according to the axial angular momentum J_z of the Bloch functions. We choose this classification because the eigenfunction analysis in terms of the heavy-hole, light-hole, and split-off character (according to J and J_z) is not adequate for structures with C_{2v} symmetry, like the dot molecule, since J is not a good quantum number. For the forthcoming analysis we only consider contributions in Eq. (13) from the first conduction band and the topmost three valence bands, so N_B equals eight (two conduction bands and six valence bands). The six valence-band contributions are divided into two $J_z = 3/2$ states, which are exactly equivalent to the heavy-hole states, and four $J_z = 1/2$ states. The four $J_z = 1/2$ states are further split into states with $|x\rangle$, $|y\rangle$ valence-band character and states with $|z\rangle$ valence-band character. We define

$$J(xy) \text{ for } \frac{|x\rangle - i|y\rangle}{\sqrt{2}}\uparrow, \quad \frac{|x\rangle + i|y\rangle}{\sqrt{2}}\downarrow,$$

$$J(z) \text{ for } |z\rangle\uparrow, \quad |z\rangle\downarrow. \tag{15}$$

This is a meaningful classification for the calculated structures where the z ([001]) direction is the growth direction.

Each envelope function f_n can be further expanded in terms of the axial angular momentum

$$f_n(x,y,z) = \sum_m f_n^m(r,z) \exp(im\phi)/\sqrt{2\pi}, \tag{16}$$

and the axial expansion coefficients are defined as the norm of f_n^m given by

$$a_n^{(m)} = \frac{1}{2\pi} \int \left| \int f_n(x,y,z) \exp(-im\phi) d\phi \right|^2 r dr dz. \tag{17}$$

For each single-particle wave function $\Psi(\boldsymbol{r})$, the axial expansion coefficients $a_n^{(m)}$ give the weight of the state according to its Bloch function character [heavy hole, $J(xy)$, $J(z)$, conduction band, indexed by n] and according to its axial angular momentum character (S, P, D, etc., indexed by m).

Starting from the correlated excitonic wave functions the degree of entanglement can be calculated following the definition of von Neumann. For the qubits A or B the entropy of entanglement S (Refs. 2 and 3) is given by

$$S(\Psi) = -\operatorname{Tr} \rho_A \log_2 \rho_A = -\operatorname{Tr} \rho_B \log_2 \rho_B, \tag{18}$$

where ρ_A is the reduced density matrix for qubit "A" (the electron) and ρ_B is the reduced density matrix for qubit "B" (the hole). The density matrices are calculated from the correlated CI exciton density ρ,

$$\rho = |\Psi\rangle\langle\Psi| = \sum_{h_i,e_j,h_k,e_l} A(h_i,e_j) A^*(h_k,e_l) |\Phi_{h_i,e_j}\rangle\langle\Phi_{h_k,e_l}| \tag{19}$$

$$= \sum_{h_i,e_j,h_k,e_l} \rho_{h_i e_j h_k e_l}, \tag{20}$$

where $A(h_i,e_j)$ are the CI expansion coefficients [see Eq. (11)]. ρ_A is obtained by tracing over all but one pair of indices:

$$\rho_A = \rho_{e_j e_l} = \sum_{h_i,h_k} \rho_{h_i e_j h_k e_l}. \tag{21}$$

For the maximally entangled state $S(\Psi) = 1$, while $S(\Psi) = 0$ for a nonentangled state.

The correlated excitonic wave functions can also be analyzed in terms of the probabilities to find the electron or the hole in the top or in the bottom dot. A mask operator $\hat{M}$, which selects a certain region of space (e.g., the top of bottom dot), can be applied to the single-particle electron or hole wave functions:

$$\tilde{\rho}_{e_i e_j}^{T/B} = \langle \psi_{e_i} | \hat{M}^{T/B} | \psi_{e_j} \rangle. \tag{22}$$

The excitonic density can then be written as a sum of weighted products of these projected densities:

$$\tilde{\rho}_{e_i e_j}^{T} \otimes \tilde{\rho}_{h_i h_j}^{T}, \quad \tilde{\rho}_{e_i e_j}^{T} \otimes \tilde{\rho}_{h_i h_j}^{B}, \tag{23}$$

$$\tilde{\rho}_{e_i e_j}^{B} \otimes \tilde{\rho}_{h_i h_j}^{T}, \quad \tilde{\rho}_{e_i e_j}^{B} \otimes \tilde{\rho}_{h_i h_j}^{B}. \tag{24}$$

From these densities, the four probabilities to find the electron and hole in the top or bottom dot can be calculated.

C. Strain-modified band-offset calculations

To appreciate the effect of strain on the hole states we perform strain-modified band-offset calculations. From the relaxed atomic positions—obtained using the valence force field (VFF) method—the strain field can be calculated for each atom from the deformation of its tetrahedron of nearest neighbors. The strain-modified band-offset Hamiltonian depends on the six irreducible components of the strain tensor, the three deformation potentials (hydrostatic and two uniaxial), and the spin-orbit splitting.[27] For the unstrained bulk its eigenvectors are the heavy-hole, light-hole, and split-off bands, while strain induces mixing of these three bands. The corresponding eigenstates were analyzed by giving to each solution a weight according to their character: heavy hole, $J(xy)$, and $J(z)$ [see Eq. (15)].

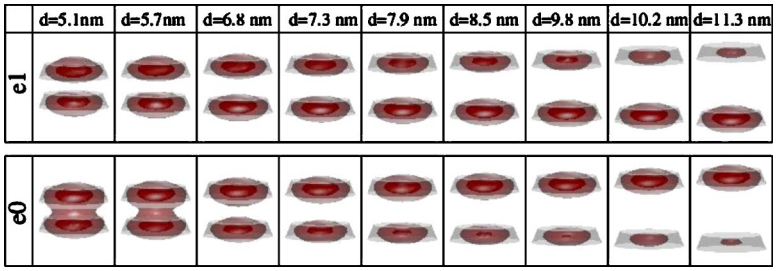

FIG. 4. (Color online) Square of the single-particle electron wave functions e_0 and e_1 for different interdot separations. The shape of the dots is given in light grey and the two isosurfaces with two different tones of dark gray (red online) contain 75% and 40% of the state densities.

III. RESULTS FOR THE SINGLE-PARTICLE STATES

A. Largely separated dots ($d \to \infty$)

Figure 1(b) shows the single-particle electron and hole energies as a function of interdot separation. For large interdot separations the single-particle hole states h_0 and h_1 are energetically almost degenerate. Figures 4 and 5 show the electron and hole wave functions as a function of the interdot separation d. In these figures, the envelope functions f_n [see Eq. (13)] averaged over eight atom cells are plotted. The physical shape of the dot (truncated cones) is shown in grey, whereas the wave functions are depicted as two isosurfaces with two shades of color enclosing 75% and 40% of the state density. The hole states h_0 and h_1 are localized on the bottom and top dots, respectively (Fig. 5). This behavior resembles H_2^+ with very long bond length where the orbitals are localized at a single atom, rather than forming a resonance.

For the single-particle electron states e_0 and e_1 the wave functions (Fig. 4) are mainly localized on the top and bottom dots, respectively. The energy splitting between these states [Fig. 1(b)] reflects the effect of alloy fluctuations, fully taken into account in our calculations, which make both dots somewhat dissimilar even if $d \to \infty$. These local fluctuations result in a lifting of the degeneracy by 3.1 meV for e_0 and e_1 and 0.2 meV for h_0 and h_1 (energy values taken from our largest interdot distance of 22.6 nm). Thus, for large interdot separations, a diatomic dot made of truncated-cone shaped constituents is not equivalent to a homonuclear diatomic molecule ($D_{2\infty}$ symmetry like H_2), but rather to a heteronuclear molecule (D_{2d} symmetry like HF). Figures 6(a) and 6(b) give the qualitative picture where for the electron and the hole the "molecular" single- particle orbitals (MO's) are constructed like for a heteronuclear molecule; i.e., the characters of the MO's are dominated by one of the single-particle states. This is justified by the fact that, at large and intermediate (i.e., for distances larger than 8 nm) interdot separations, the hopping matrix element for holes t_h is negligible while the one for electrons t_e is small (this will be shown quantitatively in Sec. V) compared to the "polarization energy" of the molecule, V_p ($2V_p \simeq e_0 - e_1 = 3.1$ meV for $d \to \infty$).

B. Closely spaced dots

We see in Fig. 4 that the electron states e_0 and e_1 form bonding-antibonding pairs as suggested by Eq. (1), whereas the hole states h_0 and h_1 (Fig. 5) do not, forming instead

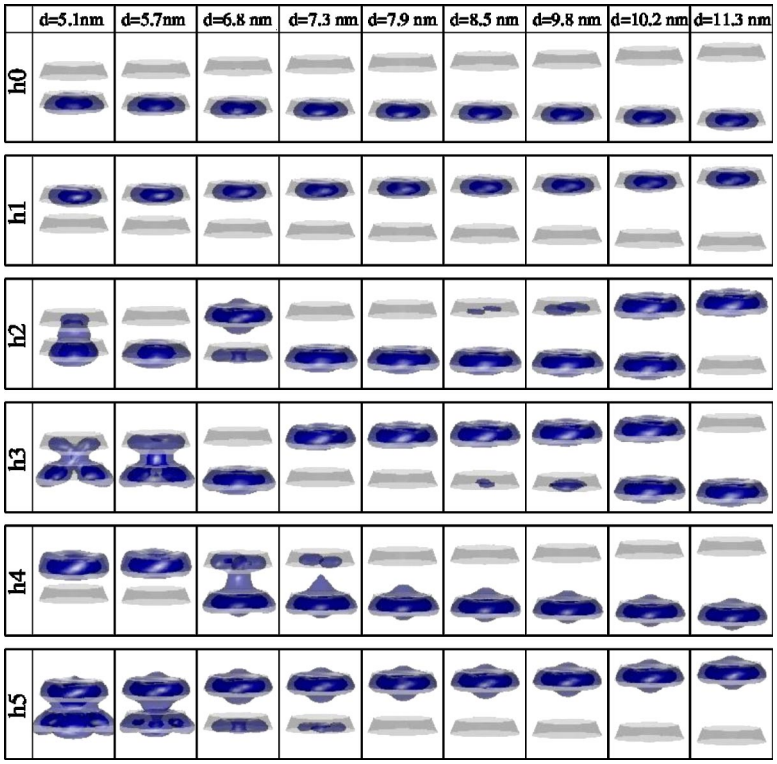

FIG. 5. (Color online) Square of the single-particle hole wave functions h_0, h_1, h_2, h_3, h_4 and h_5, for different interdot separations. The shape of the dot is given in light grey and the two isosurfaces with two different tones of dark gray (blue online) contain 75% and 40% of the state densities.

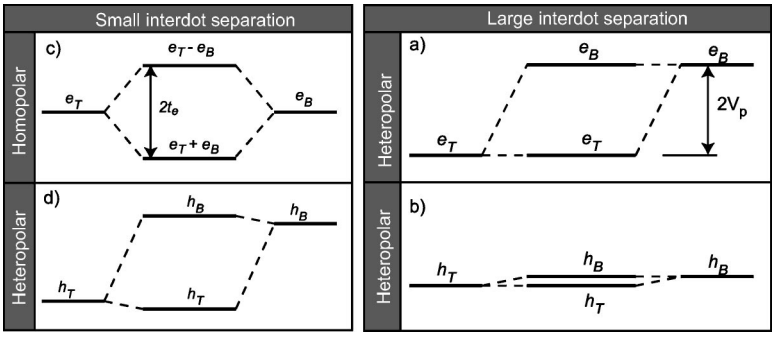

FIG. 6. Formation of single-particle "molecular orbitals" (MO's) [in the central part of panels (a), (b), (c), (d)] from the single-particle "atomic orbitals" [on the left and right sides of panels (a), (b), (c), (d)]. For large interdot separation the electrons and the hole form heteronuclearlike MO's. For small separation the electrons form bonding-antibonding combinations like homonuclear MO's.

symmetry-broken (heteronuclearlike) states. Figures 6(c) and 6(d) show this hybrid behavior where electrons form symmetric-antisymmetric combinations of MO's, akin to a homonuclear dimer, while holes give rise to heteronuclear MO's localized on one or the other dot. There are two reasons for this behavior, explained in the following two paragraphs.

1. Hole states experience a high barrier that suppresses interdot tunneling

The first reason for the broken-symmetry hole behavior is the high barrier between the two dots experienced by the heavy-hole component (dominant) of the hole states. To appreciate these facts we performed strained modified band offsets calculations (Sec. II C) for different interdot separations. Figure 7 shows the results for the first two hole confining potentials for three different interdot separations. The character [heavy hole, $J(xy)$, and $J(z)$] of each eigenstate is represented by a certain symbol of size proportional to the weight of the character. The heavy-hole confining potential is the relevant quantity for the energetics of the hole states since hole states are to over 80% heavy hole like. Examination of the heavy-hole confining potential (circles in Fig. 7) reveals that the potential is *negative* in the region of the barrier, strongly repelling heavy holes. This high barrier was also reported[28] for pure InAs truncated-pyramid dots. Furthermore, the effective barrier felt by the hole states increases upon reduction of the interdot separation, suppressing tunneling and the ability for holes to form bonding-antibonding states. Figure 1(b) also shows that the hole states move to lower energy when the interdot separation is reduced, in agreement with the increasing barrier height between the dots.

2. Due to the lack of inversion symmetry between the dots, the bottom dot is more favorable for holes

The lack of inversion symmetry between nonspherical (e.g., lens-shaped) dots leads to heteronuclear hole states. This can be seen in the top panel of Fig. 7 where indeed the confinement potential experienced at the base of the *top* dot is different than that experienced at the base of the *bottom* dot. Figure 1(b) shows that the hole states h_0 and h_1, which are energetically almost degenerate at large interdot separation, split when the distance is reduced, showing an increasing preference for holes to be in the bottom dot with diminishing interdot separation. This can be understood using a simple strain picture like given in Fig. 8. A single truncated-cone or truncated-pyramid dot with homogeneous composition is nearly unstrained on the apex while it is stained at the base. The top right panels of Fig. 8 show a cubical unit cell for the unstrained case and an elongated parallelepiped for the case of biaxial strain. The heavy holes prefer the highly strained region near the base and localize preferentially in

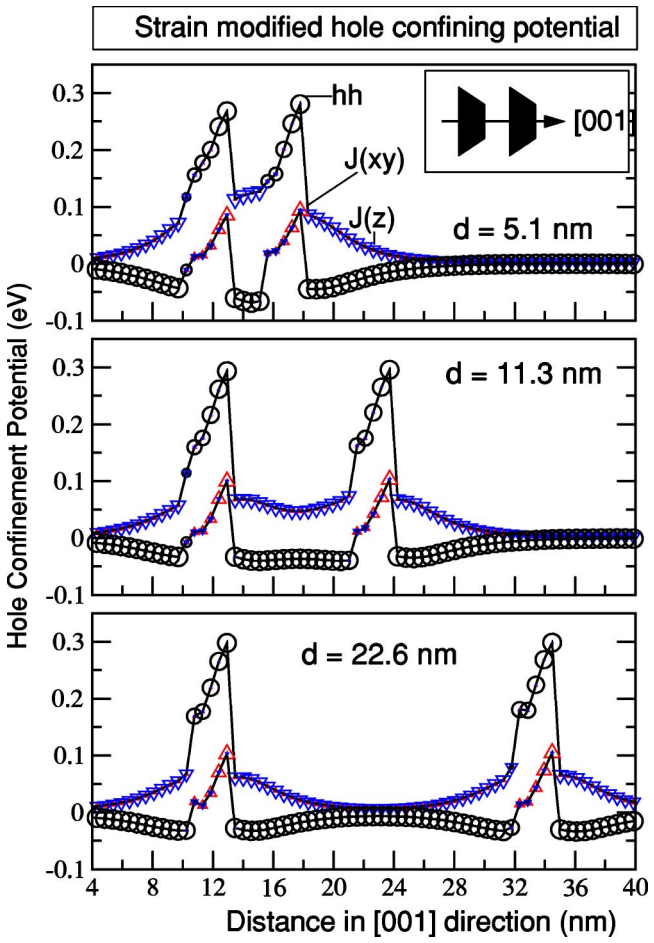

FIG. 7. Strain-modified confining potential for holes along the growth direction (001) (given in the inset of the top panel) for three dot molecules with a base-to-base separations of 5.1, 11.3, and 22.6 nm. Each data point is an average over the results obtained in the the (001) plane. The size of the circles is proportional to the weight of the heavy-hole contributions; the sizes of the triangles pointing upward [downward] are proportional to the weight of the $J(xy)$ [$J(z)$] contributions.

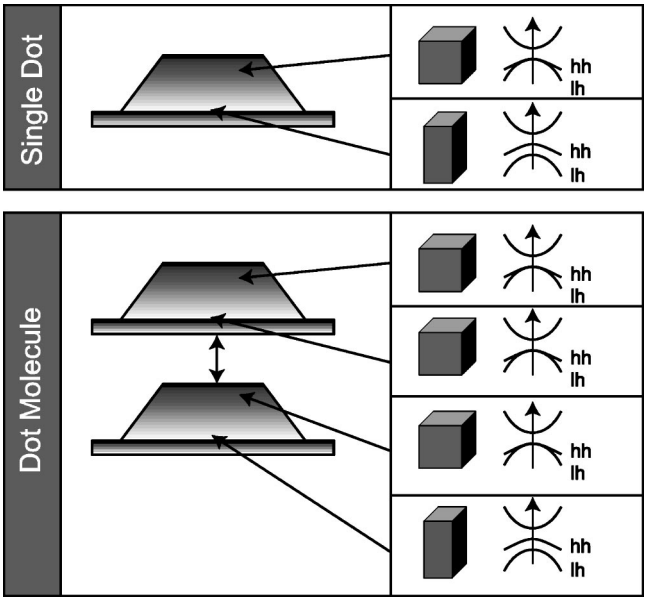

FIG. 8. Qualitative picture of the strain in a truncated-cone and in a truncated-cone molecule. The deformation of the unit cell at the base and the apex of the dot is schematically given with the corresponding strained bulk band structure. The base of the single dot and the base of the *bottom* dot (for the dot molecule) is shown to be more favorable for heavy holes.

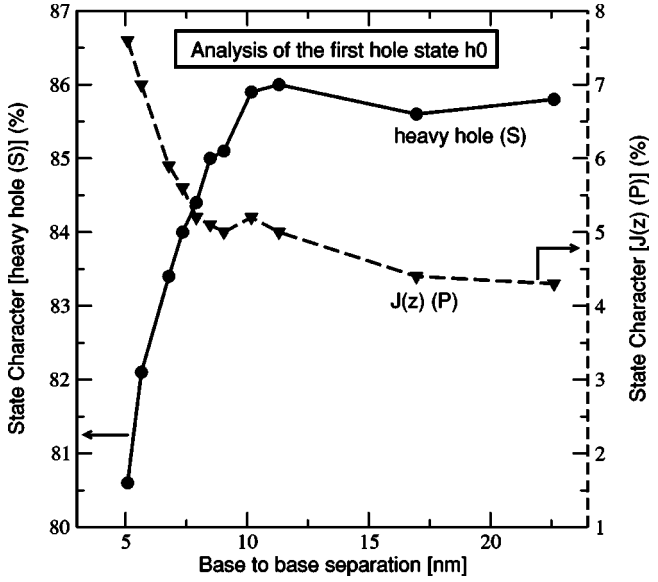

FIG. 9. Analysis of the first hole state h_0 in terms of the axial angular momentum J_z (see text) and the orbital character of the envelope functions as a function of the interdot separation. Only the heavy-hole contributions with orbital S character and $J(z)$ with orbital P character are shown.

this region as suggested by the strained bulk band structure given on the right side of Fig. 8. When two dots are close together the strain at the top but also at the base of the upper dot is almost hydrostatic due to the compression of the dot through the sandwiched material. The base of the lower dot, however, experiences biaxial strain and remains favorable for heavy holes. The magnitude of this effect should be stronger for pure InAs dots since it experiences more strain than our alloyed InGaAs dot. With a very strong preference for hole states to localize on the bottom dot, not only the first (like on our case), but the first few hole states might localized on the bottom dot. This expected behavior has been reported by Sheng and Leburton[28] performing eight band $\mathbf{k}\cdot\mathbf{p}$ calculations of a pure InAs truncated-pyramid dot molecule where the first two single-particle hole states are localized on the bottom dot. Such a localization might have detrimental consequences for the achievement of entanglement.

3. Component of the hole wave function responsible for the hole tunneling has P symmetry

Figure 7 shows how the $J(z)$ confinement potential (triangles pointing downwards) becomes attractive between the dots at small interdot separation. The effect of this attractive potential on the hole state h_0 is shown in Fig. 9, where the single-particle hole state h_0 of our pseudopotential calculation is decomposed according to its Bloch—and envelope function—character [see Eq. (17)]. Only the main contributions—the symmetric heavy-hole state with pure S envelope function and the antisymmetric $J(z)$ state with pure P envelope function—are shown. Figure 9 shows that when the interdot distance is reduced, the heavy-hole character diminishes while the $J(z)$ character increases. This is in agreement with the qualitative picture given by the strained-modified band-offset calculation where the $J(z)$ confining potential becomes attractive between the dots at small interdot separation. The part of the (multiband) wave function responsible for the hole tunneling is therefore antisymmetric P like with Bloch function character $J(z)$. This will have consequences on the optical properties described in Sec. IV showing a dark exciton state below the bright exciton state. We underline at this point that the proper treatment of hole tunneling (and therefore of all optical properties and entanglement) requires a multiband treatment like eight-band $\mathbf{k}\cdot\mathbf{p}$,[28] tight-binding,[29] or our pseudopotential approach and cannot be accounted for by single-band effective-mass approaches.[30,31]

IV. RESULTS FOR THE MANY-PARTICLE EXCITON STATES AND THE OPTICAL SPECTRUM

The energies of the four lowest exciton states formed from the single-particle states above are shown in Fig. 2(c) where the dot size is proportional to the oscillator strength. To characterize the excitonic wave functions we have calculated the probability to find both particles in the top dot (e_Th_T), both particles in the bottom dot (e_Bh_B), and the particles in different dots (e_Bh_T, e_Th_B) for each excitonic wave function. The results are given for the first four excitons in the top four panels of Fig. 10. Different symbols have been used for different occupations. The integration in Eq. (22) is performed over the volume above (top dot) and below (bottom dot) the equidistant plane between both dots. We next discuss the salient features of the exciton energies and the optical spectrum.

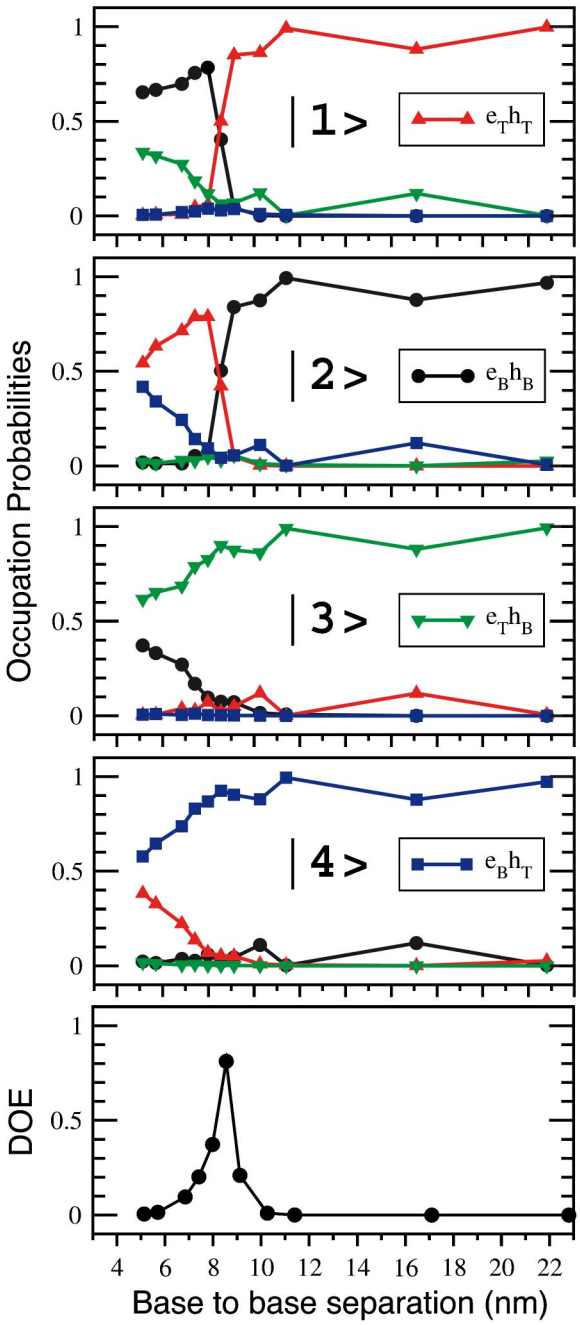

FIG. 10. Upper panels: localization of the first four exciton states numbered with increasing energy as $|1\rangle$, $|2\rangle$, $|3\rangle$, $|4\rangle$, as a function of the interdot distance. On each panel, four lines describe the occupation probability to find the electron and the hole both on the bottom dot (e_Bh_B), both on the top dot (e_Th_T), the electron on the top and the hole on the bottom (e_Th_B), and the electron on the bottom and hole on the top dot (e_Bh_T). Lower panel: entropy of entanglement as a function of the base-to-base dot separation.

A. Largely separated dots

Figure 10 shows that the excitons $|1\rangle$ and $|2\rangle$ are localized on the top and bottom dots, respectively. The states $|3\rangle$ and $|4\rangle$ are dissociated excitons where the electron and hole are localized on different dots. The excitons are therefore simple

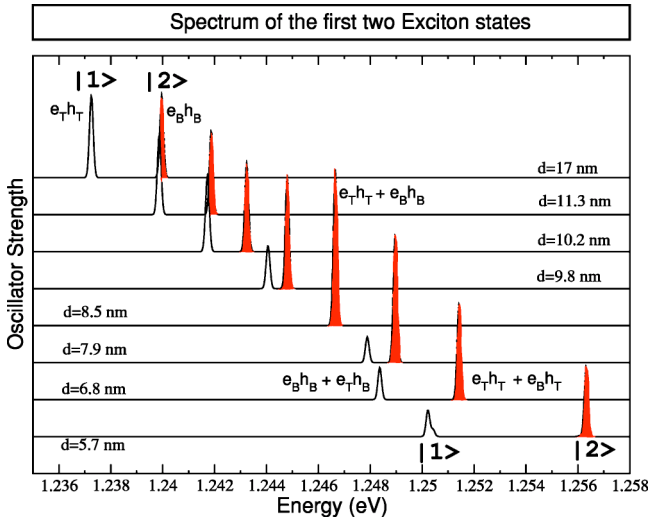

FIG. 11. Excitonic spectrum for the first two exciton states $|1\rangle$ and $|2\rangle$ as a function of the interdot separation d.

products of the single-particle molecular orbitals given in Figs. 6(a) and 6(b): $|e_Th_B\rangle$, $|e_Th_T\rangle$, $|e_Bh_B\rangle$, and $|e_Bh_T\rangle$. The on-site electron-hole Coulomb attraction U lowers the energy of the $|e_Th_T\rangle$ and $|e_Bh_B\rangle$ excitons, leading to the energetic order given in Fig. 3: $|e_Th_T\rangle$, $|e_Bh_B\rangle$, $|e_Th_B\rangle$, and $|e_Bh_T\rangle$. The $|e_Th_T\rangle/|e_Bh_B\rangle$ excitons are separated from $|e_Th_B\rangle/|e_Bh_T\rangle$ by the on-site Coulomb attraction while $|e_Bh_B\rangle$ is separated from $|e_Th_T\rangle$ (and $|e_Th_B\rangle$ from $|e_Bh_T\rangle$) by the polarization energy $2V_p$. An interesting effect is already revealed at this point: although the material properties (composition, shape, size) of both dots are identical, their exciton energies are different, as can be seen from the existence of two optically active lines in the spectrum of Fig. 2(c) for large interdot separation. Naturally, if the two dots would have different sizes or compositions, as is often the case during growth, even greater dot inequivalence will ensue.

B. Merging of the excitons $|1\rangle$ and $|2\rangle$: A many-body effect

Figure 11 shows in more detail the calculated spectrum of the fist two excitons $|1\rangle$ and $|2\rangle$ as a function of the interdot distance. When the interdot distance is reduced from 17 nm to 8.5 nm both excitonic peaks move to higher energy and move closer together until only one exciton peak is observed at $d=8.5$ nm. The diminishing energy difference between $|1\rangle$ and $|2\rangle$ is an excitonic effect. To appreciate this fact we plotted in Fig. 12 the electron-hole single-particle energies: $|TT\rangle=e_0-h_1$, $|BB\rangle=e_1-h_0$, $|BT\rangle=e_1-h_1$, and $|TB\rangle=e_0-h_0$. At large interdot separation where the excitons $|1\rangle$, $|2\rangle$, $|3\rangle$, and $|4\rangle$ (including two-body effects) are almost pure $|e_Th_T\rangle$, $|e_Bh_B\rangle$, $|e_Th_B\rangle$, and $|e_Bh_T\rangle$ the comparison between $|TT\rangle$, $|BB\rangle$, $|BT\rangle$, and $|TB\rangle$ (Fig. 12) and $|1\rangle$, $|2\rangle$, $|3\rangle$, and $|4\rangle$ [Fig. 2(c)] is meaningful. $|TT\rangle$ and $|BB\rangle$ move apart while $|1\rangle$ and $|2\rangle$ move together when d is reduced, showing the excitonic nature of the latter effect which can be understood as follows: At the single-particle level we saw in Sec. III B that the increasingly repulsive barrier for the heavy holes with decreasing interdot separation lowers the single-particle hole

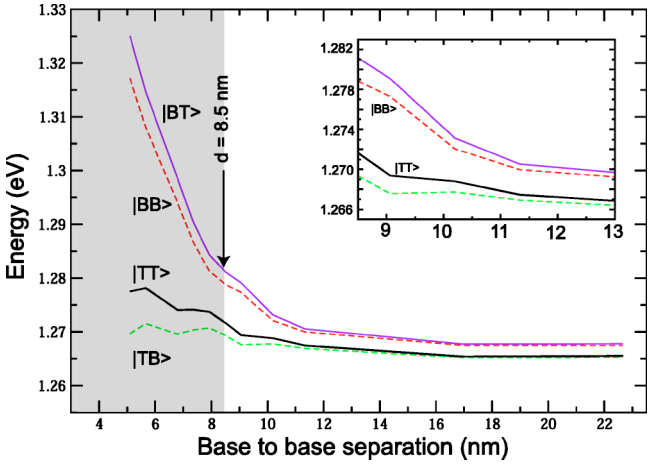

FIG. 12. Differences between single-particle electron and hole energies: $|TT\rangle = e_0 - h_1$, $|BB\rangle = e_1 - h_0$, $|BT\rangle = e_1 - h_1$, and $|TB\rangle = e_0 - h_0$. The denomination $|TT\rangle$, $|BB\rangle$, $|TB\rangle$, and $|BT\rangle$, where T stands for top and B for bottom, is only meaningful outside the shaded area, for large interdot separations, since the single-particle electron states at short base-to-base separations are neither top nor bottom.

energies [Fig. 1(b)]. This destabilization goes along with delocalization of these states. With decreasing interdot distance, the single-particle electron state e_0 becomes delocalized as well, but for another reason: it creates a bonding state with increased occupation probability between the dots (Fig. 4). Both the delocalization of the electron state e_0 and the delocalization of the hole states h_0 and h_1 contribute to lower the e-h Coulomb attractions U_{eh}^{TT} and U_{eh}^{BB}. The delocalization of the excited hole state h_1 (localized on top) is stronger than the delocalization of h_0. The magnitude of U_{eh}^{TT} is therefore reduced more severely than U_{eh}^{BB} with decreasing d. This shift is an excitonic effect which is missed by theories restricted to the single-particle level.[28,32]

C. Anticrossing of $|1\rangle$ and $|2\rangle$ at d_c: Bonding-antibonding exciton splitting

At the critical distance d_c the energy difference between $|1\rangle \simeq |e_T h_T\rangle$ and $|2\rangle \simeq |e_B h_B\rangle$ is very small, allowing them to form bonding and antibonding excitons $|e_T h_T\rangle + |e_B h_B\rangle$ and $|e_T h_T\rangle - |e_B h_B\rangle$ as shown in the "critical d" column of Fig. 3. The energy difference between these excitons is 0.4 meV and is conceptionally very similar to the Davydov splitting[33] observed in molecular crystals. Since the excitons $|e_T h_T\rangle$ and $|e_B h_B\rangle$ are highly symmetric, their bonding and antibonding combinations should yield highly symmetric and antisymmetric excitons with strong entanglement. A quantitative analysis of the entanglement will be given subsequently. Interestingly the antibonding combination (optically dark) is energetically below the bonding combination (optically bright). This is due to the fact that the single-particle hole states do not form an $ss\sigma$ bond, like the electron, but a weak $pp\sigma$ bond[34] (which will lead to a negative hopping parameter t_h in Sec. V) as described in Sec. III B 3. From a molecular point of view this situation is unexpected since dimers with electric dipoles of the excitons align "head to tail" show a bight state below the dark state. In our solid state analogous, the two "molecules" are coupled via strain and yield the unexpected "head-to-head" alignment typical of dark states below bright states in dimers.

D. Closely spaced dots: Forbidden transitions become allowed

The mixed heteronuclear and homonuclear behavior of holes and electrons, as given in Figs. 6(c) and 6(d), gives rise to excitonic states that are combinations of single-dot localized excitons $(|e_T h_T\rangle, |e_B h_B\rangle)$ and dissociated excitons $(|e_T h_B\rangle, |e_B h_T\rangle)$ (Fig. 10). These combinations are given in Fig. 3 where electrons are obviously building bonding-antibonding states and holes remain top or bottom localized. At small d all the excitons are neither symmetric nor antisymmetric and all are, to some extent, bright. This can be seen in Fig. 2(c) where the states $|3\rangle$ and $|4\rangle$ start to gain some oscillator strength as marked by the small dots visible for base-to-base separations smaller than 8 nm. These states were optically inactive (dark) at large interdot separation since electrons and holes were located on different dots forming purely dissociated states (see Figs. 10 and 3).

E. Degree of entanglement as a function of distance

The calculated degree of entanglement is given in the lower panel of Fig. 10. We see that it reaches the maximum value of 0.8 for a distance of $d_c = 8.5$ nm and decays strongly for larger or shorter distances. From this result it is obvious that a judicious choice of interdot separation is crucial for quantum computation applications. Especially the fact that small distances show unentangled states is surprising. Entanglement is a result of a fine balance between the energetic of the two dots and the electron and hole interdot coupling. Both of these quantities depend on the interdot separation as well as from the material properties of the dot. Simple models which assume a high-symmetry Hamiltonian like the theories presented in the Introduction or introduced in Refs. 11–14 naturally yield maximally entangled wave functions. The calculation as well as the measurement of the entanglement requires the treatment of atomistic effects (alloy fluctuation), strain, and correlations.

F. Exciton dissociation energy

The energy difference between states $|1\rangle$ and $|2\rangle$ (electron and hole on one dot) and $|3\rangle$ and $|4\rangle$ (electron and hole on different dots) is the exciton dissociation energy.[35,36] Figure 2(c) shows that our calculated dissociation energy is $\sim$20 meV, and it reaches its minimum value at $d = 8.5$ nm. The value of 20 meV is considerably smaller than what was found in colloidal CdSe dots (150–300 meV),[35,36] and suggests that photoconductivity has a low activation energy in self-assembled dot molecules.

G. Theoretical vs experimental spectra

In the recent experiments of Somintac *et al.*[37] and He *et al.*[38] a blueshift of the photoluminescence (PL) has been observed with decreasing interdot distance, in agreement with

our results. Earlier, Migliorato *et al.*[39] reported a redshift of the ensemble PL for stacks of vertically aligned quantum dots. Our predicted blueshift only applies to quantum dots separated by enough buffer material to still be distinct entities. The limiting case of a base-to-base separation equal to the dot height naturally yields a redshift typical of the formation of one single larger quantum dot. The theoretical results for the magnitude of the splitting of the bright states $|2\rangle$ and $|3\rangle$ in Fig. 2(c) are in good agreement with the experiments.[11–14] The agreement is even better if a systematic error of 1 nm between the interdot separation given in the experiments and the calculated base-to-base separation is assumed. We then compare the theoretical results: 42.1, 32.8, 24.8, and 16.8 meV (for the separations 5.1, 5.7, 6.8, and 7.9 nm) with the experimental 42, 30, 17, and 12 meV (for the separations 6, 7, 8, and 9).[11–14] However, unlike what is reported in the experiment, we find that the bright states are split which leads to four allowed excitons. In the case of our calculation, the appearance of four states is due to the random alloy fluctuations and the strain which affects the electronic properties of both dots and make them dissimilar. In the experiment we would expect the dots to be even more dissimilar, since the growth conditions for the top and bottom dots are different, and four peaks at short interdot distance should be observed. It is, however, conceivable to observe only two peaks at small interdot separation and one peak at large interdot separation when both dots have the same excitonic ground-state energy. This is expected to be the exception rather than the rule but might have been the case in Refs. 11, 13, and 14.

V. DISTANCE-DEPENDED TIGHT-BINDING FIT

The pseudopotential CI results can be fitted to the tight-binding parameters of Eq. (3) and yield the on-site matrix elements $\{\varepsilon_e^T, \varepsilon_e^B, \varepsilon_h^T, \varepsilon_h^B\}$, the hopping parameters $\{t_e, t_h\}$, and the electron-hole Coulomb matrix elements $\{U_{eh}^{TT}, U_{eh}^{TB}, U_{eh}^{BT}, U_{eh}^{BB}\}$ presented in Fig. 13. The analytic expressions for the distant-dependent parameters are given in Table I. We note several physical observations: (i) The on-site energies for the top and bottom dots are different, especially for holes. The difference $\varepsilon_e^T \neq \varepsilon_e^B$ and $\varepsilon_h^T \neq \varepsilon_h^B$ comes from strain effects and random alloy fluctuation, as discussed in Sec. IV. The difference decreases at $d \to \infty$, but is still present for electrons. (ii) On-site energies ε_e and ε_h depend on the interdot separation distance because of strain coupling. (iii) The electron and hole hopping parameters are well fit by exponentials Ae^{-d/d_0}. This is consistent with tunneling. We find similar tunneling depths d_0 for electrons (2.15 nm) and holes (3.64 nm), but the hole prefactor $A_h = -4.25$ is much smaller than the electron prefactor $A_e = -255$ meV. (iii) The magnitude of the on-site Coulomb energy decreases (from −29 meV to −26 meV), while the interdot interaction is $1/\epsilon_{\text{eff}} d_{\text{eff}}$, where the effective distance $d_{\text{eff}} = \sqrt{d^2 + \Delta^2}$ reflects a charge spread Δ of about 4 nm. The prefactor of approximately 100 in the interdot interaction is an effective dielectric constant around 14.5, expressed in meV and nm.

In light of these results it is obvious that the starting assumption about the on-site and hopping matrix elements adopted in the introduction and in Refs. 11, 13, and 14 is not justified. The energetic of the hole versus electron states with varying distance turns out to be very different, calling for a separate treatment of electrons and holes which might lead to a breaking of the symmetry of the *exciton* states. The electron states follow bonding-antibonding behavior while the holes keep, up to the smallest interdot distance, their top-bottom character. This difference in the behavior of electrons and holes is related to the different potential barriers experienced by the electron and the holes, as shown in Sec. III, and to their different effective masses. This is reflected by the very different tunneling matrix elements in Fig. 13. The electron and hole states are not only different because of their tunneling properties but also because of the way they react to the intrinsic properties of the dot. The single-particle energy of the electron states located on two well-separated top and bottom dots is different by about 3 meV. The same energy difference for the hole states is almost zero. For these reasons, a more elaborate model is necessary and is now, due

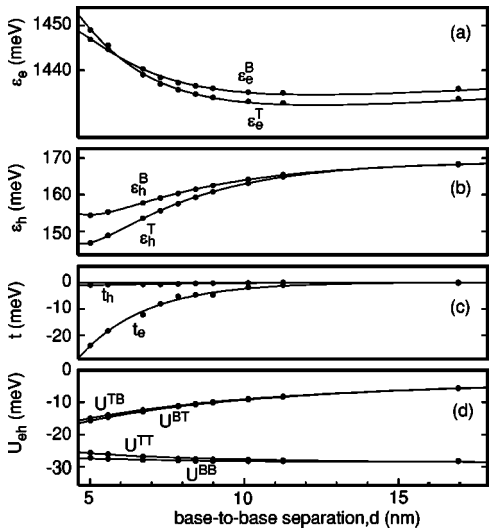

FIG. 13. Effective parameters for the two-site Hamiltonian H [Eq. (3)], distilled from our many-body pseudopotential calculation. The lines are a parametrized fit to our data points, listed in Table I.

TABLE I. Parametrization of the distance dependence of our effective two-site Hamiltonian, Eq. (3). These functions are plotted as solid lines in Fig. 13.

Parameter (meV)	Distance dependence (d in nm)
ε_e^T	$-1450-436d^{-1}+3586d^{-2}-7382d^{-3}$
ε_e^B	$-1449-452d^{-1}+3580d^{-2}-6473d^{-3}$
ε_h^T	$167+129d^{-1}-2281d^{-2}+6582d^{-3}$
ε_h^B	$163+274d^{-1}-3780d^{-2}+9985d^{-3}$
t_e	$-255\exp(-d/2.15)$
t_h	$-4.25\exp(-d/3.64)$
U_{eh}^{BB}	$-29.0+7.98/d$
U_{eh}^{TT}	$-29.6+19.6/d$
U_{eh}^{BT}	$-99.1/\sqrt{d^2+(3.72)^2}$
U_{eh}^{TB}	$-98.5/\sqrt{d^2+(4.21)^2}$

the detailed results of the pseudopotential-CI calculations and the derived tight-binding picture, possible to derive.

VI. SUMMARY

We have shown that the proper theoretical treatment of excitons in dot molecules requires an accurate description on the single-particle level (multiband coupling and strain effects must be taken into account; single-band approaches miss the qualitative picture) as well as on the few-particle level. We showed that simplified high-symmetry models commonly used in the literature yield qualitatively erroneous results.

At short interdot separations, the single-particle physics of the electron states is close to the one of a homonuclear dimer where the orbitals form bonding and antibonding states. The hole states remain, even at short interdot distance, localized on one or the other dot. We showed that the hole behavior can be explained by (i) strain, which inhibits the tunneling, and (ii) the lack of inversion symmetry between self-assembled quantum dots. This hybrid homo-nuclear-heteronuclear behavior of electrons and holes leads to four optically allowed excitons with low degree of entanglement.

At large interdot separation, both the electron and hole behave like a heteronuclear molecule forming two bright and two dark excitonic states, all four unentangled.

At a critical distance of 8.5 nm (for our dots) we predict an anticrossing of the two bright excitons accompanied by a high degree of entanglement (80%) of these states. We show that a many-body effect derived from strain is responsible for the energetic alignment of these two exciton states. At the point of energetic alignment, the excitons from bonding and antibonding exciton states. The lower energy states is shown to be antisymmetric and therefore optically dark.

In the last section we use our many-body CI results to parametrize a 4×4 tight-binding Hamiltonian and give analytic expressions for the parameters. These parameters could be used by others to model self-assembled quantum dot molecules.

ACKNOWLEDGMENTS

This work was supported by the DOE Office of Science, Basic Energy Sciences, Division of Material Sciences under Contract No. DE-AC36-99GO10337.

[1] D. Loss and D. P. DiVincenzo, Phys. Rev. A **57**, 120 (1998).
[2] C. H. Bennett and D. P. DiVincenzo, Nature (London) **404**, 247 (2000).
[3] M. A. Nielsen and I. L. Chuang, *Quantum Computation and Quantum Information* (Cambridge University Press, Cambridge, England, 2000).
[4] D. Bimberg, M. Grundman, and N. N. Ledentsov, *Quantum Dots Heterostructures* (Wiley, New York, 1999).
[5] P. I. Tamborenea and H. Metiu, Europhys. Lett. **53**, 776 (2001).
[6] G. W. Bryant and W. Jaskolski, Physica E (Amsterdam) **13**, 293 (2002).
[7] P. Zhang, X.-G. Li, and X.-G. Zhao, Phys. Lett. A **294**, 108 (2002).
[8] A. Imamoglu, D. D. Awschalom, G. Burkard, D. P. DiVincenzo, D. Loss, M. Sherwin, and A. Small, Phys. Rev. Lett. **83**, 4204 (1999).
[9] D. P. DiVincenzo, D. Bacon, J. Kempe, G. Burkard, and K. B. Whaley, Nature (London) **408**, 339 (2000).
[10] D. Loss and E. V. Sukhorukov, Phys. Rev. Lett. **84**, 1035 (2000).
[11] M. Bayer, P. Hawrylak, K. Hinzer, S. Fafard, M. Korkusinski, Z. R. Wasilewski, O. Stern, and A. Forchel1, Science **291**, 451 (2001).
[12] K. Hinzer, M. Bayer, J. P. McCaffrey, P. Hawrylak, M. Korkusinski, O. Stern, Z. R. Wasilewski, S. Fafard, and A. Forchel, Phys. Status Solidi B **224**, 385 (2001).
[13] M. Bayer, G. Ortner, A. Larionov, V. Timofeev, A. Forchel, P. Hawrylak, K. Hinzer, M. Korkusinski, S. Fafard, and Z. Wasilewski, Physica E (Amsterdam) **12**, 900 (2002).
[14] M. Korkusinski, P. Hawrylak, M. Bayer, G. Ortner, A. Forchel, S. Fafard, and Z. Wasilewski, Physica E (Amsterdam) **13**, 610 (2002).
[15] G. S. Solomon, J. A. Trezza, A. F. Marshall, and J. S. Harris, Phys. Rev. Lett. **76**, 952 (1996).
[16] D. M. Bruls, P. M. Koenraad, H. W. M. Salemink, J. H. Wolter, M. Hopkinson, and M. S. Skolnick, Appl. Phys. Lett. **82**, 3758 (2003).
[17] M. Bayer, A. Kuther, A. Forchel, A. Gorbunov, V. B. Timofeev, F. Schafer, J. P. Reithmaier, T. L. Reinecke, and S. N. Walck, Phys. Rev. Lett. **82**, 1748 (1999).
[18] J. Shumway, A. J. Williamson, A. Zunger, A. Passaseo, M. DeGiorgi, R. Cingolani, M. Catalano, and P. Crozier, Phys. Rev. B **64**, 125302 (2001).
[19] C. Pryor, J. Kim, L.-W. Wang, A. J. Williamson, and A. Zunger, J. Appl. Phys. **83**, 2548 (1998).
[20] G. Bester, J. Shumway, and A. Zunger, Phys. Rev. Lett. **93**, 047401 (2004).
[21] A. Franceschetti, H. Fu, L.-W. Wang, and A. Zunger, Phys. Rev. B **60**, 1819 (1999).
[22] L.-W. Wang and A. Zunger, Phys. Rev. B **59**, 15 806 (1999).
[23] P. N. Keating, Phys. Rev. **145**, 637 (1966).
[24] A. J. Williamson, L.-W. Wang, and A. Zunger, Phys. Rev. B **62**, 12 963 (2000).
[25] A. L. Fetter and J. D. Walecka, *Quantum Theory of Many-Particle Systems* (McGraw-Hill, New York, 1971).
[26] R. Resta, Phys. Rev. B **16**, 2717 (1977).
[27] S.-H. Wei and A. Zunger, Phys. Rev. B **49**, 14 337 (1994).
[28] W. D. Sheng and J. P. Leburton, Appl. Phys. Lett. **81**, 4449 (2002).
[29] W. Jaskolski, M. Zielinski, and G. W. Bryant, Physica E (Amsterdam) **17**, 40 (2003).
[30] C. D. Simserides, U. Hohenester, G. Goldoni, and E. Molinari, Phys. Status Solidi B **224**, 745 (2001).
[31] C. D. Simserides, U. Hohenester, G. Goldoni, and E. Molinari, Phys. Rev. B **62**, 13 657 (2000).

[32] W. D. Sheng and J. P. Leburton, in *Compound Semiconductors 2001*, Institute of Physics Conference Series (IOP, Bristol, 2002), pp. 513–518.
[33] D. P. Craig and S. H. Walmsley, *Excitons in Molecular Crystals* (Benjamin, New York, 1968).
[34] J. Slater and G. Koster, Phys. Rev. **94**, 1498 (1954).
[35] A. Franceschetti and A. Zunger, Phys. Rev. B **63**, 153304 (2001).
[36] C. A. Leatherdale, C. R. Kagan, N. Y. Morgan, S. A. Empedocles, M. A. Kastner, and M. G. Bawendi, Phys. Rev. B **62**, 2669 (2000).
[37] A. Somintac, E. Estacio, and A. Salvador, J. Cryst. Growth **251**, 196 (2003).
[38] J. He, Y. C. Zhang, B. Xu, and Z. G. Wang, J. Appl. Phys. **93**, 8898 (2003).
[39] M. A. Migliorato, L. R. Wilson, D. J. Mowbray, M. S. Skolnick, M. Al-Khafaji, A. G. Cullis, and M. Hopkinson, J. Appl. Phys. **90**, 6374 (2001).